OPEN

NPG Asia Materials (2015) 7, e157; doi:10.1038/am.2014.126

www.nature.com/am

ORIGINAL ARTICLE

Highly flexible and robust N-doped SiC nanoneedle field emitters

Shanliang Chen[1,2], Pengzhan Ying[2], Lin Wang[1], Guodong Wei[1], Fengmei Gao[1], Jinju Zheng[1], Minhui Shang[1], Zuobao Yang[1], Weiyou Yang[1] and Tom Wu[3]

Flexible field emission (FE) emitters, whose unique advantages are lightweight and conformable, promise to enable a wide range of technologies, such as roll-up flexible FE displays, e-papers and flexible light-emitting diodes. In this work, we demonstrate for the first time highly flexible SiC field emitters with low turn-on fields and excellent emission stabilities. *n*-Type SiC nanoneedles with ultra-sharp tips and tailored N-doping levels were synthesized via a catalyst-assisted pyrolysis process on carbon fabrics by controlling the gas mixture and cooling rate. The turn-on field, threshold field and current emission fluctuation of SiC nanoneedle emitters with an N-doping level of 7.58 at.% are 1.11 V μm^{-1}, 1.55 V μm^{-1} and 8.1%, respectively, suggesting the best overall performance for such flexible field emitters. Furthermore, characterization of the FE properties under repeated bending cycles and different bending states reveal that the SiC field emitters are mechanically and electrically robust with unprecedentedly high flexibility and stabilities. These findings underscore the importance of concurrent morphology and composition controls in nanomaterial synthesis and establish SiC nanoneedles as the most promising candidate for flexible FE applications.
NPG Asia Materials (2015) **7,** e157; doi:10.1038/am.2014.126; published online 23 January 2015

INTRODUCTION

Flexible electronic devices have attracted extensive attention in recent decades because of their numerous promising applications, such as flexible energy-storage devices, wearable energy-harvesting systems and stretchable electronics.[1–4] Among the emerging technologies, there is considerable interest in flexible field emission (FE) emitters due to their unique lightweight, conformable and flexible nature, which give them the significant advantage of being utilized in roll-up flexible FE displays,[3] e-papers[5] and high-performance X-ray tubes.[6] To enable such next-generation flexible devices, flexible cathodes must be used as the fundamental starting component to replace conventional emitters grown on rigid substrates. These flexible emitters should maintain their original or even better FE properties as well as excellent electrical and mechanical performances after bending, compressing, twisting and stretching.[7,8] To date, a variety of cathodes have been developed based on flexible substrates such as polymers,[9] graphene[7] and carbon fabrics.[10] However, material- and fabrication-related obstacles to the realization of high-performance flexible emitters remain.

Silicon carbide (SiC) is an excellent material candidate for constructing advanced FE emitters. SiC is a third-generation wide band-gap semiconductor with excellent physical properties such as high strength and stiffness, high-temperature stability, corrosion resistance and high thermal conductivity.[11–13] To date, several studies have explored the FE properties of nanostructured SiC emitters grown on rigid substrates. Particularly, the reported turn-on fields (E_{to}, defined as the electric field required to generate a current density of 10 μA cm^{-2}) of SiC nanowires are in the range of 3.33–20 V μm^{-1},[14–17] and those of SiC nanorods and nanobelts are 13–17 V μm^{-1},[18] and 3.2 V μm^{-1},[19] respectively. E_{to} can be further reduced to 0.7–2.9 V μm^{-1} by using aligned SiC nanowires as emitters.[20,21] However, there have been few studies focusing on flexible SiC field emitters.[22–24] Furthermore, there have been no investigations of the effect of doping on the crystal growth behavior of SiC one-dimensional (1D) nanostructures or their FE properties. The aim of this study is to explore flexible SiC field emitters with low E_{to}, high performance and good stability, and there is a particularly urgent need for insight into the mechanical and electrical robustness of flexible SiC field emitters under different stresses.

In the present study, we investigate the N-doping controlled growth of *n*-type SiC nanoneedles on carbon fabrics, producing highly flexible and robust SiC field emitters. To significantly enhance the FE properties of SiC emitters, we have developed strategies to leverage the local field enhancement effect by precisely controlling the growth of SiC nanoneedles with sharp tips[25] and to increase the localized density of states at the Fermi level by incorporating suitable dopants.[24,26] The obtained SiC nanoneedles exhibit excellent properties with low E_{to} in a narrow range of 1.11–1.38 V μm^{-1}, excellent electron emission stability and high flexibility as well as unprecedented

[1]Institute of Materials, Ningbo University of Technology, Ningbo, China; [2]School of Material Science and Engineering, China University of Mining and Technology, Xuzhou, China and [3]Materials Science and Engineering, Physical Sciences and Engineering, King Abdullah University of Science and Technology (KAUST), Thuwal, Saudi Arabia
Correspondence: Dr W Yang or Dr T Wu, Materials Science and Engineering, Physical Sciences and Engineering, King Abdullah University of Science and Technology (KAUST), Thuwal 23955-6900, Saudi Arabia.
E-mail: weiyouyang@tsinghua.org.cn or tao.wu@kaust.edu.sa
Received 25 July 2014; revised 11 October 2014; accepted 17 November 2014

mechanical and electrical robustness. Our work establishes such N-doped SiC nanoneedles as the most promising candidate for application to practical flexible FE devices.

EXPERIMENTAL PROCEDURE

Flexible *n*-type SiC nanoneedles were synthesized by catalyst-assisted pyrolysis of polysilazane precursor (Supplementary Figure S1, Institute of Chemistry, Chinese Academic of Science, China) on the substrates of carbon fabrics in a conventional graphite-heater furnace. First, the liquid polysilazane was solidified by heat treatment at 260 °C for 30 min in a quartz tube furnace under Ar atmosphere (purity: 99.99%) and then ball-milled into amorphous SiCN(O) powders. Carbon fabric substrates were immersed in an ethanolic solution of $Co(NO_3)_2$ with a concentration of 0.05 mol l^{-1} for 2 min and then dried in air naturally at room temperature. The treated substrates were placed on the top of a graphite crucible (purity: 99%) containing 300 mg of the SiCN(O) powders. Subsequently, the crucible with the substrate was positioned in the center of the graphite-heater furnace. The furnace chamber was first pumped to 10^{-4} Pa, and an N_2/Ar gas mixture (both N_2 and Ar of 99.99% purity, 0.1 MPa) was then introduced into the chamber. The gas purge was repeated for three times to reduce the O_2 content in the chamber to a negligible level. Finally, the furnace was heated to the desired temperature of 1450 °C within 48 min and then cooled to 1100 °C within various times of 25, 35 and 40 min under different cooling rates, followed by natural cooling to room temperature. To control the doping levels of SiC 1D nanostructures during the pyrolysis process, different N_2/Ar gas mixtures with various N_2 contents of 5, 10 and 15 vol% were introduced into the furnace chamber with a flowing rate of 200 sccm. The as-synthesized samples, S1, S2, S3, S2-1 and S3-1, refer to the products fabricated with cooling times of 25 min, 25 min, 25 min, 35 min and 40 min and N_2 contents of 5 vol%, 10 vol%, 15 vol%, 10 vol% and 15 vol% within the gas mixtures, respectively.

The obtained products were characterized using FE scanning electron microscopy (FE-SEM, S-4800, Hitachi, Tokyo, Japan), high-resolution transmission electron microscopy (high-resolution TEM, JEM-2100F, JEOL, Kawagoe, Japan) equipped with energy dispersive X-ray spectroscopy (Quantax-STEM, Bruker, Karlsruhe, Germany), X-ray diffraction (D8 Advance, Bruker) with Cu Ka radiation ($\lambda = 1.5406$ Å) and X-ray photoelectron spectroscopy (AXIS ULTRA DLD, Shimadzu, Kyoto, Japan). The FE properties of flexible *n*-type SiC nanoneedles with exposed areas of 0.4×0.4 cm^2 were measured in a home-built high-vacuum setup with a base pressure of $\sim 1.5 \times 10^{-7}$ Pa at room temperature. The current–voltage (*I*–*V*) curves were recorded on a Keithley 248 meter (Tektronix, Cleveland, OH, USA) with a detection resolution of 0.1 fA. The distance between the surface of the SiC nanoneedle emitter and the anode of the vacuum chamber was fixed at ~700 μm.

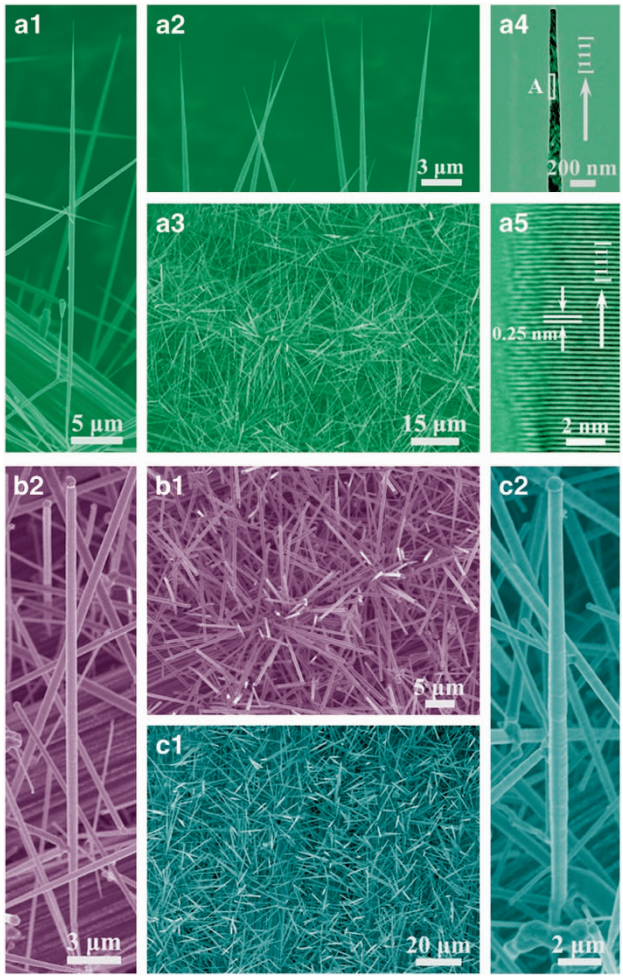

Figure 1 (**a1**–**a3**) Typical scanning electron microscopy (SEM) images of a SiC nanoneedle of sample S1 under different magnifications. (**a4**) Typical transmission electron microscopy (TEM) image of a SiC nanoneedle. (**a5**) High-resolution TEM image recorded from the marked area A in **a4**. (**b1**, **b2**) SEM images of the SiC nanowire of sample S2 under different magnifications. (**c1**, **c2**) SEM images of the SiC nanowire of sample S3 under different magnifications.

RESULTS

To synthesize 1D SiC nanostructures with controlled doping, the volume ratio of gas mixture N_2/Ar in the pyrolysis procedure was carefully tailored at 5:95, 10:90 and 15:85. The cooling rate was kept constant as 14 °C min^{-1} as the temperature decreased from 1450 to 1100 °C. The obtained products are denoted samples S1, S2 and S3, respectively.

Figures 1a1–a3 shows representative SEM images of sample S1 grown on a carbon fabric substrate under different magnifications, suggesting the large-scale and homogeneous growth of 1D nanostructures on the substrate (see also Supplementary Figures S2a and b). The density of SiC nanostructures is $\sim 3.6 \times 10^5$ mm^{-2} based on SEM observations. Notably, the nanostructures are needle-like and have clear and sharp tips (Figures 1a1 and a2). The typical length of nanoneedles is ~40 μm, with an average aspect ratio of ~65 (Figure 1a1). Figure 1a4 shows a typical TEM image of a SiC nanoneedle, revealing a tapered morphology with a smooth surface and a tiny tip sized ~35 nm on average. Figure 1a5 shows the corresponding high-resolution TEM image of the needle recorded from the marked area of A in Figure 1a4. The distance between two fringes is ~0.25 nm, corresponding to the {111} planes of 3*C*-SiC, suggesting that the nanoneedle grows along the [111] direction. The selected area electron diffraction pattern of the SiC nanoneedle (Supplementary Figure S2c) confirms that the 3*C*-SiC nanoneedle has a single-crystalline nature. The average concentration of N dopants is ~4.39 at.% with a uniform spatial distribution, based on the measurements of >20 nanoneedles (Supplementary Figure S2d), suggesting that the nanoneedles are *n*-type SiC.[27]

Figures 1b1, b2 and c1, c2 shows typical SEM images of samples S2 and S3 under different magnifications, respectively. Interestingly, unlike the needle-shaped nanowires of sample S1, conventional SiC nanowires without sharp tips were obtained (Supplementary Figures S3 and S4), implying that the compositions of gas mixtures exert a profound effect on the growth morphology of the SiC nanostructures. Catalyst droplets on the heads of wires in samples S2 and S3 are often observed. The energy dispersive X-ray spectroscopy spectrum recorded from the droplet reveals a composition of mostly Si, C, Co and Cu (the Cu signal arises from the copper grid used to support the TEM

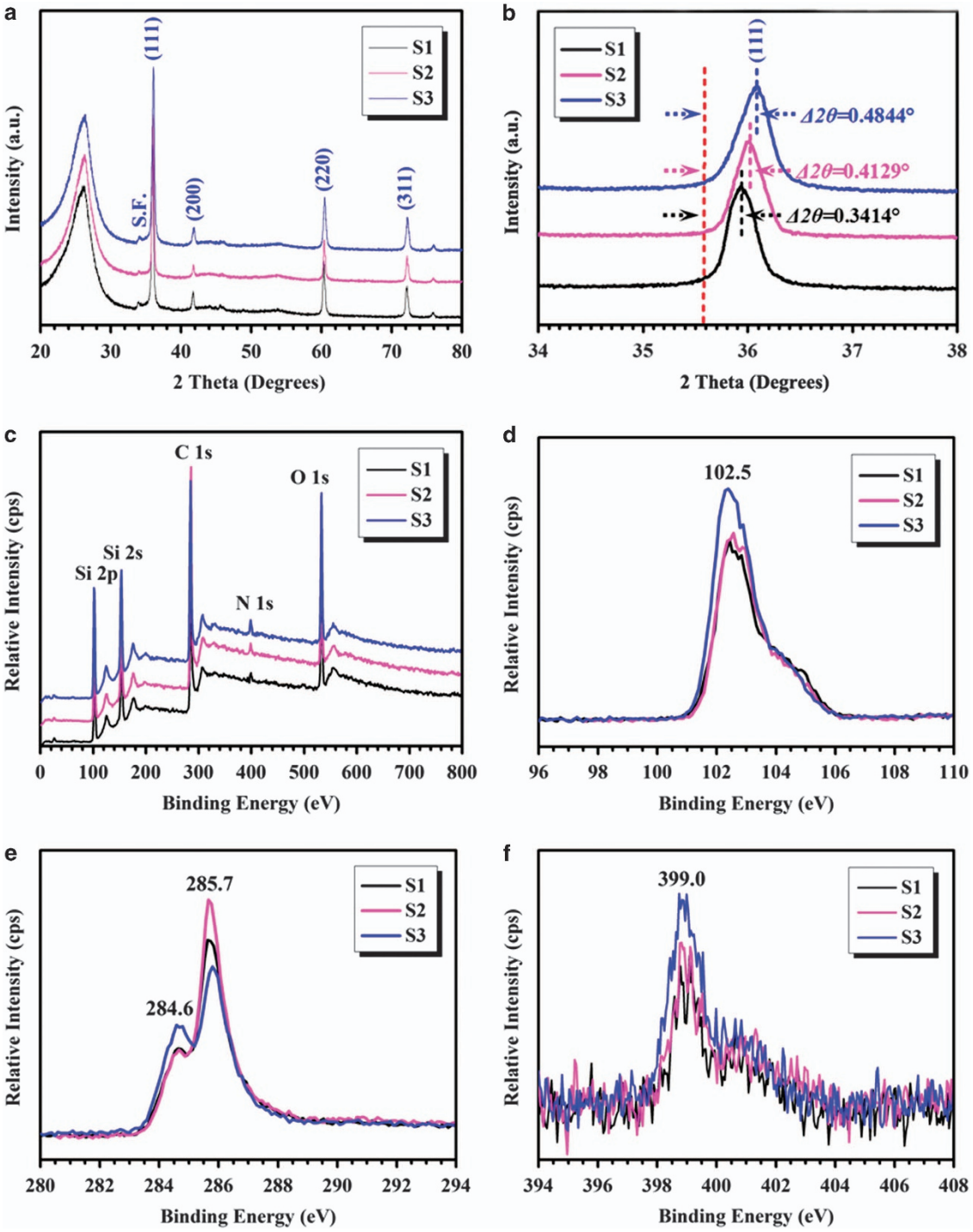

Figure 2 (**a**) X-ray diffraction patterns of samples S1, S2 and S3. (**b**) Enlarged view showing the shift of (111) diffraction peaks as a result of different N-doping levels. (**c**) Survey XPS spectra, along with the spectra of (**d**) Si 2p, (**e**) C 1s, and (**f**) N 1s.

sample), as shown in Supplementary Figure S5, suggesting that the growth of the wires is dominated by a vapor-liquid-solid mechanism. The catalyst droplets have typical sizes of ~500 nm and ~700 nm for samples S2 and S3, respectively (Figures 1b2 and c2, Supplementary Figures S3 and S4). The nanowires are also 3C-SiC with similar single crystallinity and [111] growth direction as sample S1, regardless of the composition of gas mixtures used during growth (Supplementary Figures S3c and d). The average concentrations of N dopants in samples S2 and S3 are ~5.78 at.% and 7.32 at.%, respectively. These results suggest that the morphologies and N-doping levels of SiC nanoneedles can be concurrently tailored by adjusting the ratio of N_2/Ar in the gas mixture (see Supplementary Figure S6 for the proposed mechanism for doping-controlled growth of SiC nanowires).

Figures 2a and b show the X-ray diffraction patterns of as-synthesized samples S1, S2 and S3. Peaks in Figure 2a can be indexed to diffraction from SiC (111), (200), (220) and (311) planes,

indicating that the as-grown products are pure 3*C*-SiC (JCPDS Card No. 29-1129). The peak marked with 'S.F.' is ascribed to the stacking faults within 3*C*-SiC.[28] Figure 2b presents a closer view of (111) peaks. Compared with the standard data (JCPDS Card No. 29-1129), which is marked as a red dashed line, the (111) peaks of all samples shift to higher angles, suggesting the successful N-doping of the SiC nanostructure in the form of a substitutional solid solution.[27] The higher N-doping levels would lead to more lattice distortions of 3*C*-SiC, which consequently causes larger shifts of the (111) peaks, as observed in samples S1, S2 and S3. This trend is consistent with the N-doping levels of ~4.39 at.%, 5.78 at.% and 7.32 at.% in samples S1, S2 and S3, respectively, as derived from energy dispersive X-ray spectroscopy analyses.

Further evidence for N-doping in the SiC nanoneedles is provided by the X-ray photoelectron spectroscopy data shown in Figures 2c–f. The binding energies are standardized for specimen charging using C 1s as the reference at 284.6 eV. Figure 2c shows the survey spectra of samples S1, S2 and S3, and no other elements except Si, C, N and O are observed. The O peak mainly rises from oxygen absorbed on the surfaces of SiC nanostructures. The Si 2p and C 1s features are shown in Figures 2d and e, respectively. The peaks centered at ~102.5 eV and ~285.7 eV are attributed to Si 2p and C 1s of SiC, respectively.[29] Furthermore, the Si 2p peak in Figure 4d exhibits an asymmetric shape with a tail at higher binding energy, which can be ascribed to SiO_x species on the nanoneedle surfaces.[30] The spectrum in Figure 2e displays another C 1s peak at a lower binding energy of ~284.6 eV, which is the signal of the carbon fabrics. In Figure 2f, N 1s peaks centered at ~399.0 eV are clearly observed, confirming N-doping in the crystal lattices of SiC nanostructures.

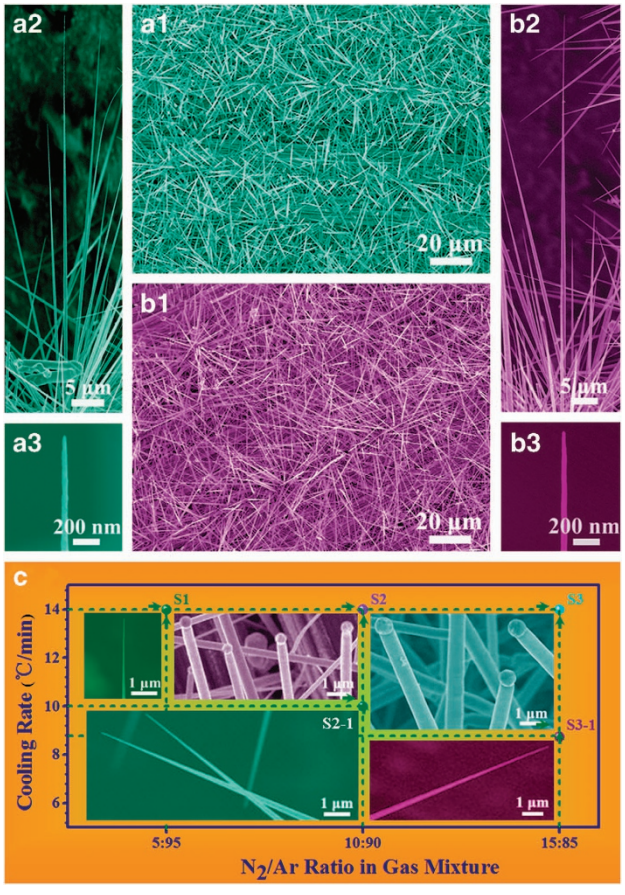

Figure 3 (**a1**–**a3**) Typical scanning electron microscopy (SEM) images of the SiC nanoneedle in sample S2-1 under different magnifications. (**b1**–**b3**) SEM images of the SiC nanoneedle of sample S3-1 under different magnifications. (**c**) Summary of the SiC nanostructures, that is, nanoneedles and nanowires, as a function of gas mixture and cooling rate applied during the synthesis.

N-doping strongly influences the FE performance of 1D semiconductor nanostructures.[31,32] To investigate the N-doping-level-dependent FE properties of SiC nanostructures, emitters with comparable morphology should be used; in this case, sharp tips should be maintained. Based on our previous work on the controlled growth of SiC field emitters,[33] we prepared SiC nanoneedles by prolonging the cooling time from 1450 to 1100 °C to 35 and 40 min (that is, cooling rates fixed at 10 °C min^{-1} and 8.75 °C min^{-1}, respectively) with otherwise identical experimental conditions as samples S2 and S3, and the obtained samples are denoted samples S2-1 and S3-1, respectively. Figures 3a1–a3 and b1–b3 show typical SEM images of samples S2-1 and S3-1 under different magnifications, respectively, revealing the successful synthesis of SiC nanoneedles with sharp and clear tips. The average diameter of the needle tips for both samples is ~35 nm, which is comparable to that of sample S1. The N-doping levels of samples S2-1 and S3-1 are ~6.01 at.% and 7.58 at.%, respectively.

The experimental results of samples S1, S2, S3, S2-1 and S3-1 suggest that both the doping level and the morphology of *n*-type SiC can be reliably controlled by tailoring the N_2/Ar ratio in the gas mixtures and the cooling rate during the pyrolysis process. Particularly, the growth of high-quality SiC nanoneedles with tailored N-doping levels could be accomplished by using lower cooling rates. These concurrent controls, shown in Figure 3c, offer unprecedented opportunities to explore the FE functionalities of SiC nanostructures.

We next explore how the N-doping level affects the FE properties of SiC nanoneedles. The experimental setup used for the FE measurements is shown in Supplementary Figure S7. We chose samples S1, S2-1 and S3-1 (that is, with similar sharp-tip structures and different N-doping levels of 4.39, 6.01 and 7.58 at.%) for the investigation. Figure 4a shows FE current density (*J*) as a function of applied field (*E*). The *J*–*E* curves are obtained after sweeping the voltage several times until the electron emission becomes stable. The relatively smooth and consistent *J*–*E* curves imply that the SiC nanoneedles of the three samples all exhibit excellent stability during field-induced electron emission. These nanoneedles are quite robust, and no change in morphology was detected after FE measurements (Supplementary Figure S8). According to the recorded *J*–*E* plots, the turn-on fields of S1, S2-1 and S3-1 are 1.38 V μm^{-1}, 1.22 V μm^{-1} and 1.11 V μm^{-1}, respectively, with threshold fields (E_{thr}, defined as the electric field required to generate a current density of 1 mA cm^{-2}) of 1.79 V μm^{-1}, 1.64 V μm^{-1} and 1.55 V μm^{-1}, respectively (Figure 4b). Both the E_{to} and E_{thr} data suggest slight decreases with increased N-doping levels. The E_{to} and E_{thr} values obtained here are among the highest reported for flexible cold cathodes based on carbon cloth substrates, underscoring the excellent FE performance of the present *n*-type SiC nanoneedles. For comparison, the performance parameters of other SiC nanostructure-based field emitters on rigid substrates, as well as some typical inorganic semiconductor emitters, are shown in Supplementary Table S1. The significant performance enhancement of our SiC nanoneedles could be attributed to both the sharp-tip morphology and N-doping. The sharp tips facilitate the local field effect enhancement for field-induced electron emission[26,34] and ensure the absence of catalyst particles on the tips.[33] Meanwhile, N-doping improves the conductivity of the emitters, resulting in superior FE

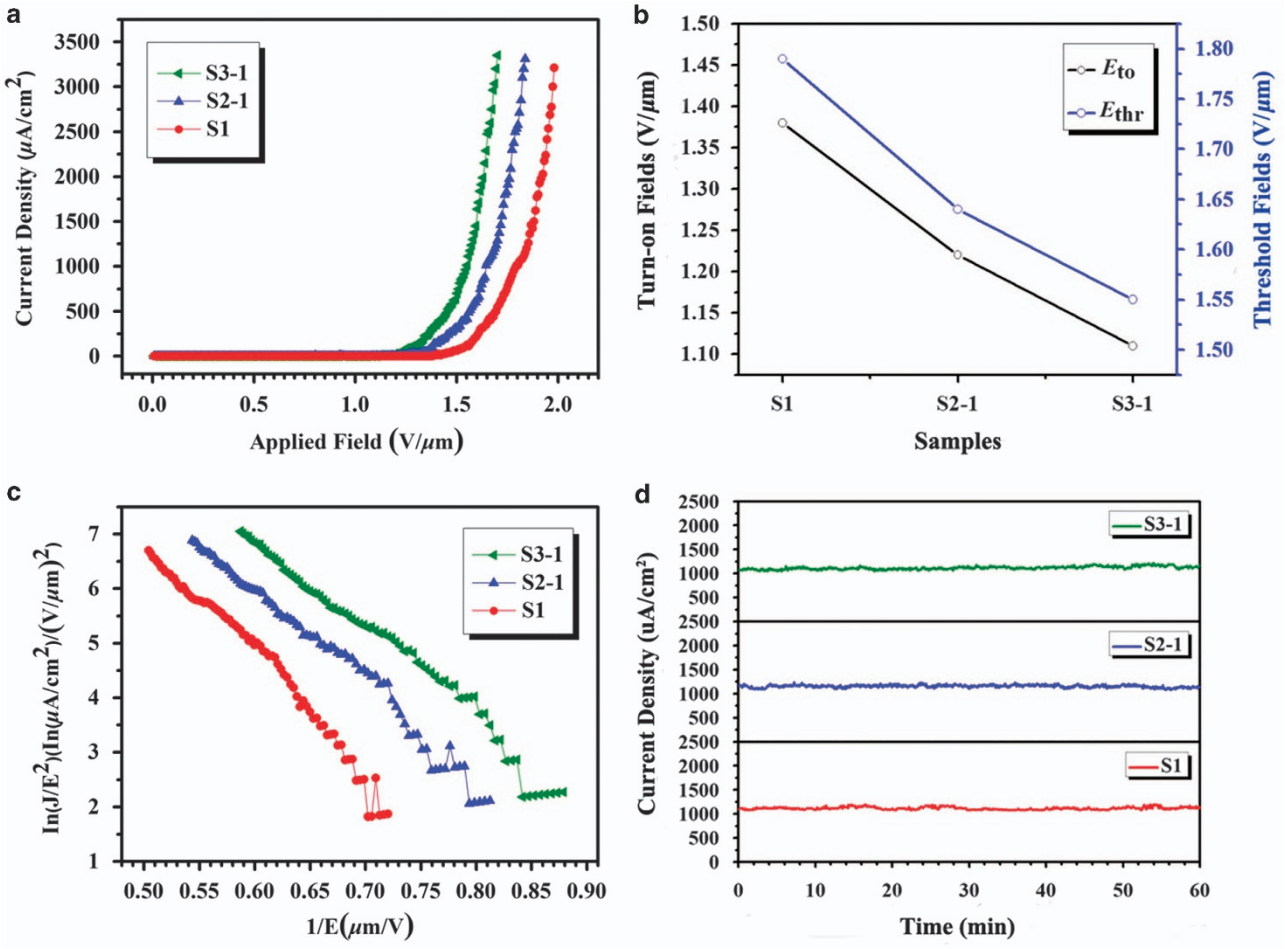

Figure 4 (**a**) *J–E* curves of the SiC nanoneedle of samples S1, S2-1 and S3-1, respectively. (**b**) E_{to} and E_{thr} data for samples S1, S2-1 and S3-1. (**c**) F–N plots for samples S1, S2-1 and S3-1. (**d**) Field emission stabilities of samples S1, S2-1 and S3-1.

performance.[32] N-doping favors the formation of localized impurity states near the conduction band edge and reduces the work function, improving electron FE.[23,24]

To better understand the FE behavior, the current–voltage characteristics are expressed by the Fowler–Nordheim (F–N) equations:[35]

$$J = \left(A\beta^2E^2/\phi\right)\cdot\exp\left(-B\phi^{3/2}/\beta E\right) \quad (1)$$

or

$$\ln\left(J/E^2\right) = \ln\left(A\beta^2/\phi\right) - B\phi^{3/2}/\beta E \quad (2)$$

where E is the applied electric field, $A = 1.54\times10^{-6}\,\mathrm{eV\,V^{-2}}$, $B = 6.83\times10^{3}\,\mathrm{eV^{-3/2}\,V\,\mu m^{-1}}$, β is the field enhancement factor and ϕ is the work function of the emitter material (that is, 4.0 eV for SiC)[12]. The F–N plots corresponding to samples S1, S2-1 and S3-1, obtained by plotting $\ln(J/E^2)$ versus $1/E$, are displayed in Figure 4c. The linear relationships of the F–N plots indicate that electron emission from the SiC emitters follows the conventional FE mechanism. In addition to E_{to} and E_{thr}, FE stability is another critically important factor and should be carefully considered for field emitters. Figure 4d shows the emission stability of samples S1, S2-1 and S3-1 by recording the emission current at $J = 1138\,\mu\mathrm{A\,cm^{-2}}$ every 3 s for 60 min. Remarkably, no obvious emission degradation is observed. The current fluctuations are ~7.7%, 6.5% and 8.1% for samples S1, S2-1 and S3-1, respectively, suggesting the highly stable electron emission of the as-synthesized *n*-type SiC nanoneedles, comparable to the highest previously reported results for SiC emitters.[17,24,36] These results also reveal for the first time that the current emission stability of flexible *n*-type SiC field emitters is not sensitive to N-doping levels in the range investigated herein.

Figure 5a depicts digital photographs of sample S3-1 in various bending states. Our results reveal the high flexibility of SiC nanoneedles on carbon fabric substrates. These flexible emitters can be bended in various states more than 200 times without noticeable structural damage. To investigate the mechanical and electrical robustness of the flexible cathode, the FE properties of the flexible *n*-type SiC field emitters of sample S3-1 subjected to repeated bending and various bending states were investigated, as shown in Figures 5b–h. Figure 5b presents the *J–E* plots of sample S3-1 after bending cycles of 0, 50, 100, 150 and 200 times (bending radius: ~2 cm), which shows negligible variations of E_{to} and E_{thr}. Figure 5c provides the corresponding F–N plots, and the linear relationships reveal that electron emission after bending still follows the conventional FE mechanism. These results confirm that our synthesized SiC field emitters are mechanically and electrically robust.

To further explore the FE performance of flexible SiC field emitters, the FE properties of S3-1 were measured in concave, flat and convex

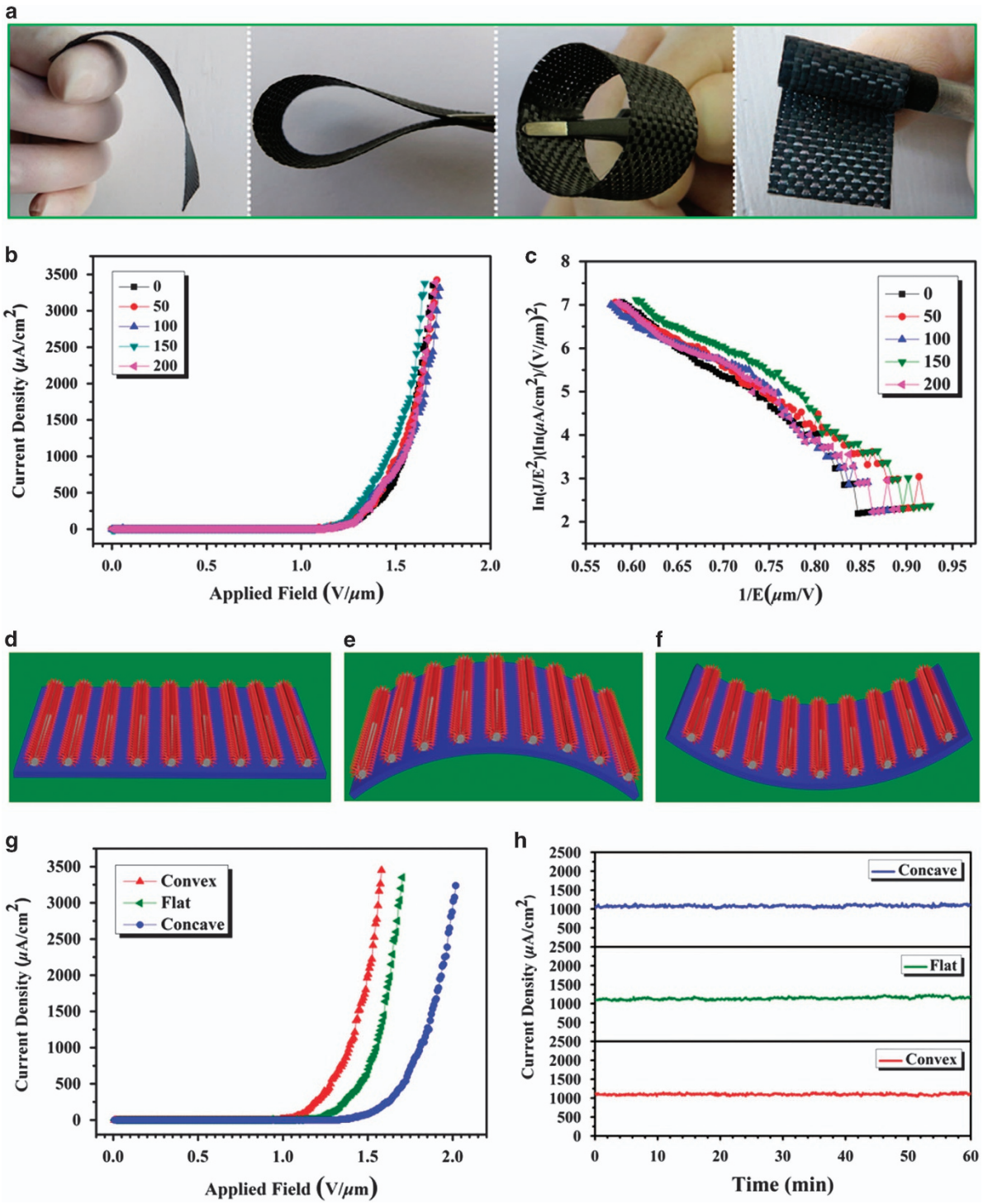

Figure 5 (**a**) Digital photographs showing the high flexibility of SiC nanoneedles grown on carbon fabric with various bended states (suspended; folded; bended with a radius of ~1.2 cm; bended with a radius of ~0.3 cm). (**b**) *J*–*E* curves and (**c**) F–N plots of sample S3-1 after 0, 50, 100, 150 and 200 bending cycles. (**d**–**f**) Schematic illustrations of sample S3-1 in concave, flat and convex states, respectively. (**g**) *J*–*E* curves of sample S3-1 in concave, flat and convex states. (**h**) Field emission stability of sample S3-1 in concave, flat and convex states.

states, which are schematically shown in Figures 5d–f. The bending radii were fixed at ~2 cm for both concave and convex geometries. Figure 5g shows the *J*–*E* curves for concave, flat and convex states, and the E_{to} and E_{thr} of sample S3-1 are ~0.98 and 1.39, 1.11 and 1.55, 1.33 and 1.81 V μm^{-1}, respectively. Both E_{to} and E_{thr} decrease monotonically in the order of concave, flat, then convex structures. Figure 5h exhibits the FE stabilities of sample S3-1 under various bending states. The current fluctuations are ~8.9%, 8.1% and 7.1% for the concave, flat and convex geometries, respectively. No noticeable emission degradation was observed, implying the

excellent FE stabilities of the synthesized flexible *n*-type SiC field emitters. Compared with their concave and flat counterparts, a slight decrease of E_{to} and E_{thr} as well as the enhancement of FE stability of SiC emitters in convex geometry could be attributed to a weaker screening effect induced by neighboring emitter sites.[7,37] No obvious change in current fluctuations was found, suggesting that the stresses of the substrate caused by different bending states do not have any significant effect on emission stability. These experimental results confirm that the present *n*-type SiC nanoneedles could be an excellent candidate for robust field emitters with high flexibility, low E_{to} and E_{thr} and high stability.

DISCUSSION

In summary, we have demonstrated for the first time the controlled growth of flexible *n*-type SiC nanoneedles with tailored N-doping levels via the catalyst-assisted pyrolysis of polymeric precursors on carbon fabric substrates. The composition of the N_2/Ar gas mixture and the cooling rate in the pyrolysis procedure concurrently exert profound effects on the growth morphology (either tapered nanoneedles or uniform nanowires) and the chemical composition of the SiC nanostructures. With the highest N-doping level of 7.58 at.%, the turn-on field is 1.11 $V\mu m^{-1}$ and the current emission fluctuation is 8.1%, suggesting that the flexible *n*-type SiC field emitters possess excellent electron emission properties. Furthermore, the obtained flexible SiC field emitters are mechanically and electrically robust when subjected to repeated bending cycles and under various bending states, confirming that the present *n*-type SiC nanoneedles are an ideal candidate for high-performance field emitters with unprecedented stability. Overall, the current work opens new doors for exploring flexible field emitters with excellent FE properties via simultaneous control of the morphologies and doping levels of 1D semiconductor nanostructures.

CONFLICT OF INTEREST

The authors declare no conflict of interest

ACKNOWLEDGEMENTS

Research reported in this publication was financially supported by the 973 program (Grant no. 2012CB326407) and the National Natural Science Foundation of China (NSFC, Grant nos. 51372122 and 51372123). This work was also supported by the King Abdullah University of Science and Technology (KAUST).

Author contributions: WY and TW conceived and directed the experiments. SC, PY, GW, FG, JZ, MS and ZY performed the experiments. SC, WY and TW co-wrote the manuscript. All authors discussed the results and helped with the preparation of the final manuscript.

1 Gwon, H., Kim, H. S., Lee, K. U., Seo, D. H., Park, Y. C., Lee, Y. S., Ahn, B. T. & Kang, K. Flexible energy storage devices based on graphene paper. *Energy Environ. Sci.* **4**, 1277–1283 (2011).
2 Wang, Z., Wang, H., Liu, B., Qiu, W., Zhang, J., Ran, S., Huang, H., Xu, J., Han, H. & Chen, D. Transferable and flexible nanorod-assembled TiO_2 cloths for dye-sensitized solar cells, photodetectors, and photocatalysts. *ACS Nano* **5**, 8412–8419 (2011).
3 Lahiri, I., Verma, V. P. & Choi, W. An all-graphene based transparent and flexible field emission device. *Carbon* **49**, 1614–1619 (2011).
4 Lai, Y. C., Huang, Y. C., Lin, T. Y., Wang, Y. X., Chang, C. Y., Li, Y., Lin, T. Y., Ye, B. W., Hsieh, Y. P. & Su, W. F. Stretchable organic memory: toward learnable and digitized stretchable electronic applications. *NPG Asia Mater.* **6**, e87. doi:10.1038/am.2013.85 (2014).
5 Comiskey, B., Albert, J., Yoshizawa, H. & Jacobson, J. An electrophoretic ink for all-printed reflective electronic displays. *Nature* **394**, 253–255 (1998).
6 Tan, T., Sim, S., Lau, S., Yang, H., Tanemura, M. & Tanaka, J. X-ray generation using carbon-nanofiber-based flexible field emitters. *Appl. Phys. Lett.* **88**, 103105 (2006).
7 Hwang, J. O., Lee, D. H., Kim, J. Y., Han, T. H., Kim, B. H., Park, M., No, K. & Kim, S. O. Vertical ZnO nanowires/graphene hybrids for transparent and flexible field emission. *J. Mater. Chem.* **21**, 3432–3437 (2011).
8 Jeong, H. J., Jeong, H. D., Kim, H. Y., Kim, S. H., Kim, J. S., Jeong, S. Y., Han, J. T. & Lee, G. Flexible field emission from thermally welded chemically doped graphene thin films. *Small* **8**, 272–280 (2012).
9 Ghosh, P., Yusop, M. Z., Satoh, S., Subramanian, M., Hayashi, A., Hayashi, Y. & Tanemura, M. Transparent and flexible field electron emitters based on the conical nanocarbon structures. *J. Am. Chem. Soc.* **132**, 4034–4035 (2010).
10 Yuan, L., Tao, Y., Chen, J., Dai, J., Song, T., Ruan, M., Ma, Z., Gong, L., Liu, K., Zhang, X., Hu, X., Zhou, J. & Wang, Z. Carbon nanoparticles on carbon fabric for flexible and high-performance field emitters. *Adv. Funct. Mater.* **21**, 2150–2154 (2011).
11 Wong, E. W., Sheehan, P. E. & Lieber, C. M. Nanobeam mechanics: elasticity, strength, and toughness of nanorods and nanotubes. *Science* **277**, 1971–1975 (1997).
12 Fang, X., Bando, Y., Gautam, U. K., Ye, C. & Golberg, D. Inorganic semiconductor nanostructures and their field-emission applications. *J. Mater. Chem.* **18**, 509–522 (2008).
13 Li, S., Wang, N., Zhao, H. & Du, L. Synthesis and electrical properties of p-type 3*C*-SiC nanowires. *Mater. Lett.* **126**, 217–219 (2014).
14 Li, Z., Li, W., Wang, X. & Zhang, M. Improving field-emission properties of SiC nanowires treated by H_2 and N_2 plasma. *Phys. Status Solidi A* **7**, 1550–1554 (2014).
15 Deng, S., Li, Z., Wang, W., Xu, N., Zhou, J., Zheng, X., Xu, H., Chen, J. & She, J. Field emission study of SiC nanowires/nanorods directly grown on SiC ceramic substrate. *Appl. Phys. Lett.* **89**, 023118–023118-3 (2006).
16 Shen, G., Bando, Y. & Golberg, D. Self-assembled hierarchical single-crystalline β-SiC nanoarchitectures. *Cryst. Growth Des.* **7**, 35–38 (2007).
17 Wong, K., Zhou, X., Au, F. C., Lai, H., Lee, C. & Lee, S. Field-emission characteristics of SiC nanowires prepared by chemical-vapor deposition. *Appl. Phys. Lett.* **75**, 2918–2920 (1999).
18 Zhou, X., Lai, H., Peng, H., Au, F. C., Liao, L., Wang, N., Bello, I., Lee, C. & Lee, S. Thin β-SiC nanorods and their field emission properties. *Chem. Phys. Lett.* **318**, 58–62 (2000).
19 Wei, G., Qin, W., Kim, R., Sun, J., Zhu, P., Wang, G., Wang, L., Zhang, D. & Zheng, K. Quantum confinement effect and field emission characteristics of ultrathin 3*C*-SiC nanobelts. *Chem. Phys. Lett.* **461**, 242–245 (2008).
20 Pan, Z., Lai, H. L., Au, F. C., Duan, X., Zhou, W., Shi, W., Wang, N., Lee, C. S., Wong, N. B. & Lee, S. T. Oriented silicon carbide nanowires: synthesis and field emission properties. *Adv. Mater.* **12**, 1186–1190 (2000).
21 Yang, Y., Meng, G., Liu, X., Zhang, L., Hu, Z., He, C. & Hu, Y. Aligned SiC porous nanowire arrays with excellent field emission properties converted from Si nanowires on silicon wafer. *J. Phys. Chem. C* **112**, 20126–20130 (2008).
22 Wu, R., Zhou, K., Wei, J., Huang, Y., Su, F., Chen, J. & Wang, L. Growth of tapered SiC nanowires on flexible carbon fabric: toward field emission applications. *J. Phys. Chem. C* **116**, 12940–12945 (2012).
23 Chen, S., Ying, P., Wang, L., Wei, G., Zheng, J., Gao, F., Su, S. & Yang, W. Growth of flexible N-doped SiC quasialigned nanoarrays and their field emission properties. *J. Mater. Chem. C* **1**, 4779–4784 (2013).
24 Zhang, X., Chen, Y., Liu, W., Xue, W., Li, J. & Xie, Z. Growth of *n*-type 3C-SiC nanoneedles on carbon fabric: toward extremely flexible field emission devices. *J. Mater. Chem. C* **1**, 6479–6486 (2013).
25 Liu, C., Hu, Z., Wu, Q., Wang, X., Chen, Y., Sang, H., Zhu, J., Deng, S. & Xu, N. Vapor-solid growth and characterization of aluminum nitride nanocones. *J. Am. Chem. Soc.* **127**, 1318–1322 (2005).
26 Zhang, X., Chen, Y., Xie, Z. & Yang, W. Shape and doping enhanced field emission properties of quasialigned 3*C*-SiC nanowires. *J. Phys. Chem. C* **114**, 8251–8255 (2010).
27 He, Z., Wang, L., Gao, F., Wei, G., Zheng, J., Cheng, X., Tang, B. & Yang, W. Synthesis of n-type SiC nanowires with tailored doping levels. *CrystEngComm* **15**, 2354–2358 (2013).
28 Koumoto, K., Takeda, S., Pai, C. H., Sato, T. & Yanagida, H. High-resolution electron microscopy observations of stacking faults in β-SiC. *J. Am. Ceram. Soc.* **72**, 1985–1987 (1989).
29 Takeshita, T., Kurata, Y. & Hasegawa, S. Bonding properties of glow-discharge polycrystalline and amorphous Si-C films studied by X-ray diffraction and X-ray photoelectron spectroscopy. *J. Appl. Phys.* **71**, 5395–5400 (1992).
30 Iwanowski, R., Fronc, K., Paszkowicz, W. & Heinonen, M. XPS and XRD study of crystalline 3*C*-SiC grown by sublimation method. *J. Alloys Compd.* **286**, 143–147 (1999).
31 Zhong, Z., Lee, G. I., Mo, C. B., Hong, S. H. & Kang, J. K. Tailored field-emission property of patterned carbon nitride nanotubes by a selective doping of substitutional N (sN) and pyridine-like N (pN) atoms. *Chem. Mater.* **19**, 2918–2920 (2007).
32 Gautam, U. K., Panchakarla, L., Dierre, B., Fang, X., Bando, Y., Sekiguchi, T., Govindaraj, A., Golberg, D. & Rao, C. Solvothermal synthesis, cathodoluminescence, and field-emission properties of pure and N-doped ZnO nanobullets. *Adv. Funct. Mater.* **19**, 131–140 (2009).

33 Chen, S., Ying, P., Wang, L., Gao, F., Wei, G., Zheng, J., Xie, Z. & Yang, W. Controlled growth of SiC flexible field emitters with clear and sharp tips. *RSC Adv.* **4**, 8376–8382 (2014).
34 Fang, X., Wu, L. & Hu, L. ZnS nanostructure arrays: a developing material star. *Adv. Mater.* **5**, 585–598 (2011).
35 Fowler, R. H. & Nordheim, L. Electron emission in intense electric fields. *Proc. R. Soc. Lond. Ser. A* **119**, 173–181 (1928).
36 Zhou, W., Wu, Y., Kong, E. S. W., Zhu, F., Hou, Z. & Zhang, Y. Field emission from nonaligned SiC nanowires. *Appl. Surf. Sci.* **253**, 2056–2058 (2006).
37 Liu, N., Fang, G., Zeng, W., Zhou, H., Long, H. & Zhao, X. Enhanced field emission from three-dimensional patterned carbon nanotube arrays grown on flexible carbon cloth. *J. Mater. Chem.* **22**, 3478–3484 (2012).

Supplementary Information accompanies the paper on the NPG Asia Materials website (http://www.nature.com/am)